

# Aerosol Optical Depth and Land Surface Reflectance From Multiangle AATSR Measurements: Global Validation and Intersensor Comparisons

William M. F. Grey, Peter R. J. North, Sietse O. Los, and Ross M. Mitchell

**Abstract**—This paper presents the results and satellite inter-comparisons for the retrieval of aerosol optical depth (AOD) and land surface bidirectional reflectance using the Multiangle Advanced Along-Track Scanning Radiometer (AATSR). The algorithm developed is based on inversion of a physical model of light scattering that requires no *a priori* knowledge of the land surface. The model is evaluated for a number of sites around the world to test its operation over a range of aerosol types and land covers including dark and bright surfaces. Validation is performed using Aerosol Robotic Network ground-based sun-photometer measurements and by intercomparison with independent estimates of AOD derived from spaceborne instruments including Multiangle Imaging Spectroradiometer (MISR), Moderate Resolution Imaging Spectroradiometer (MODIS), and Total Ozone Mapping Spectrometer (TOMS) aerosol products. Results show good agreement (Pearson's correlation coefficient  $r^2 = 0.70$  for all sites combined) between the AATSR-derived estimates of AOD and the sun-photometer measurements. There is also a high correlation ( $r^2 = 0.84$ ) between the AATSR- and MISR-derived AOD estimates, but the correlations of the AATSR-derived AOD with MODIS-derived AOD and TOMS aerosol index are lower. In addition, the ability of the sensor to discriminate between different aerosol types is evaluated. Moreover, the estimates of the aerosol properties are used for atmospheric correction of the top-of-atmosphere reflectance. The AATSR surface reflectances are compared with the MODIS bidirectional reflectance distribution function/Albedo and MISR surface products and are shown to correspond with root-mean-square errors of 0.03 and 0.06 or better, respectively. The retrieval method is applied on an image basis resulting in an image of surface reflectance and a separate map of AOD. A map of AOD at 550 nm covering the Sahel and southern Sahara region is presented to demonstrate operation at regional and potentially global scales.

**Index Terms**—Advanced Along-Track Scanning Radiometer (AATSR), aerosol optical depth (AOD), atmospheric correction, bidirectional reflectance, multiangle.

## I. INTRODUCTION

**T**HE REFLECTANCE at optical wavelengths measured by a satellite radiometer consists of solar radiation scattered

by both the surface and atmosphere in the line-of-sight of the sensor. To make full use of the information content of these top-of-atmosphere (TOA) observations, the atmospheric and surface scattering contributions of the satellite signal need to be decoupled. Obtaining the surface scattering component of the signal is necessary to allow observations to be compared over time [1] and for quantitative measurements of biophysical properties of vegetation [2]–[4]. Failure to remove the atmospheric signal results in uncertainties in derived land surface parameters and in any intercomparison of the measurements. However, retrieving the land surface bidirectional reflectance of optical data is a major problem, primarily due to the uncertainty in estimating scattering by atmospheric aerosols [5].

Aerosols have a significant impact on the Earth's climate both directly, by scattering and absorbing the incoming radiation from the sun, and indirectly, by influencing cloud formation and albedo [6], [7]. These atmospheric particles, which include both natural and anthropogenic sources, are estimated to have a net negative forcing effect on the Earth's radiation budget in the range  $-0.5$  to  $-2.5$   $\text{W/m}^2$ , which is comparable in magnitude to positive forcing caused by anthropogenic greenhouse gases ( $+2.0$  to  $+2.5$   $\text{W/m}^2$ ) [8], [9]. In addition, modification of the magnitude and directionality of the downwelling radiation is thought to have a significant role in plant photosynthesis [10], [11]. Despite the importance of the role that aerosols play in the Earth's climate forcing, they remain a major uncertainty in climate modeling [12], [13]. This is in part due to the lack of accurate and repetitive measurements at global scales [14]. Moreover, the residence time of aerosols in the atmosphere is short (of the order of a few days); consequently, their distribution and composition are highly variable. Aerosols are particularly difficult to monitor because frequent observations at global scales are required to properly characterize aerosol dynamics and their sources.

Satellite remote sensing offers a viable means for routinely measuring aerosols over very large areas. For instance, the Advanced Very High Resolution Radiometer (AVHRR) is used operationally for measuring aerosols over oceans [15], [16] but has been less successful over land where the surface is brighter and more temporally variable [17]. Another instrument that has a long-term archive of aerosol measurements is Total Ozone Mapping Spectrometer (TOMS). TOMS has been providing global observations of aerosol on a daily basis for more than 20 years. These aerosol estimates are derived using satellite radiances in the ultraviolet region and are based on a quantity

Manuscript received August 2, 2005; revised December 3, 2005. This work was supported in part by the U.K. Natural Environment Research Council under award NER/T/S/2001/00976 and in part by the Climate and Land-Surface Systems Interactions Centre.

W. M. F. Grey, P. R. J. North, and S. O. Los are with the Natural Environment Research Council Climate and Land-Surface Systems Interaction Centre, Department of Geography, University of Wales Swansea, Swansea SA2 8PP, U.K. (e-mail: w.m.f.grey@swan.ac.uk).

R. M. Mitchell is with the CSIRO Earth Observation Centre, Canberra 2601, Australia.

Digital Object Identifier 10.1109/TGRS.2006.872079

known as the aerosol index (AI). The AI is a function of aerosol optical depth (AOD) as well as single-scattering albedo and aerosol layer height and is particularly sensitive to absorbing aerosols [18], [19]. However, there are large uncertainties in the TOMS AI principally because the instantaneous field of view of the sensor is large ( $50 \times 50$  km at nadir), resulting in a high likelihood of subpixel cloud contamination [5]. Aerosol estimates from Moderate Resolution Imaging Spectroradiometer (MODIS) have also been retrieved based on spectral separation of the surface and atmospheric signal [20], [21].

Single-look approaches do not provide all the information needed for remote sensing of aerosols [5]. To address this issue, a number of instruments, such as Polarization and Directionality of the Earth's Reflectances (POLDER), Multiangle Imaging Spectroradiometer (MISR), Along-Track Scanning Radiometer (ATSR-2), and Advanced Along-Track Scanning Radiometer (AATSR), have been developed with the enhanced capability of acquiring simultaneous multiangle observations through different path lengths, allowing the atmospheric properties to be inferred. Retrievals of aerosol properties have previously been demonstrated in a number of studies based on multi-look observations of MISR [22], [23], POLDER [24], and ATSR-2 [25]–[28]. The advantage of the multilook approach over single-look methods is that assumptions are not required about the land surface spectral properties; thus, aerosols can potentially be retrieved over any surface.

In this paper, multilook AATSR measurements are used for retrieving AOD and bidirectional reflectance over land without *a priori* knowledge of land cover. AATSR was launched by the European Space Agency (ESA) onboard Envisat in March 2002 and is one of a series of satellite instruments with the purpose of providing a well-calibrated long-term global data set of satellite data for climate research [29]. To all practical intents, the instrument is identical to its predecessor, the ATSR-2 sensor launched in 1995, and provides continuity to the ATSR-1 and ATSR-2 data sets. One of the benefits of these missions is that a long time series of aerosol measurements spanning more than a decade can be obtained. The AATSR acquires two near-simultaneous observations of the same area of the Earth's surface at a viewing angle of  $55^\circ$  (forward view at the surface) and then approximately 120 s later at an angle close to vertical (nadir view). The observations made in forward view are more influenced by atmospheric scattering and absorption than in the nadir view because the path length is approximately twice that of the nadir view. The swaths are approximately 500 km wide, and the nominal size of each pixel at nadir is  $1 \times 1$  km. There are seven spectral bands, but only the four bands in the visible and near infrared (555, 660, 870, and 1610 nm) are used for aerosol retrieval. These spectral bands are narrow (approximately 20 nm) and avoid atmospheric water vapor absorption regions in the electromagnetic spectrum.

Using multiangle observations is complicated by the fact that surface bidirectional reflectance at optical wavelengths is dependent on the sun and sensor geometries. There has been continuing interest in this problem due to the need to normalize measurements acquired at a variety of sun and sensor positions [30], to obtain hemispherically integrated parameters such as

albedo [31], and to make use of information in the angular domain to improve estimates of land surface biophysical properties [32]. Variations in reflectance between simultaneous multiangular measurements of the ground are due to surface scattering in addition to the difference in atmospheric path length and scattering phase function.

To separate the atmospheric properties and surface reflectance from multiangle measurements, both the angular variations due to atmospheric effects and surface scattering need to be taken into account. To achieve this, North *et al.* [27] developed a simple physical model of light scattering that is pertinent to the dual-angle sampling of AATSR. It has been shown that estimates of AOD over land using the ATSR-2 optical channels can be retrieved using this model, but there has been very little validation of these AOD estimates. In addition, studies have been limited to local or regional areas, such as boreal forests [33] or temperate regions [34].

This paper examines the potential of the dual-angle retrieval method applied to AATSR for quantitative mapping of aerosols over different land surfaces globally. Testing is performed over a representative range of land covers, aerosol sources, latitudes, and solar and viewing geometries using ground-based sun-photometer measurements of AOD for comparison. Intersensor comparisons with the estimates of AOD derived from the MISR and MODIS instruments and with the TOMS AI product are also carried out. These AATSR-derived estimates of the aerosol properties are used for atmospheric correction of the TOA reflectance, allowing land surface bidirectional reflectance to be retrieved. The AATSR-derived surface reflectances are compared with the MODIS bidirectional reflectance distribution function (BRDF)/Albedo and MISR surface products. The dual-angle retrieval method is also applied on an image basis to a single AATSR scene. Moreover, to demonstrate that the method can potentially be implemented at a global scale and to examine spatial coherence of the results, a regional-scale map of AOD at 550 nm covering the Sahel and southern Sahara region is presented.

## II. SURFACE SCATTERING MODEL

The TOA radiance is a fraction of both the atmospheric and surface scattering. For multiangle measurements of TOA radiance, both the spectral and angular information can be used solve the inverse problem and enable separation of the atmospheric and surface scattering contributions to the observed signal. If the land surface were Lambertian, then the differences between the measured radiances from the different viewing positions could be attributed to atmospheric scattering only. However, natural surfaces are almost always anisotropic. Thus, we need to consider how the bidirectional reflectance factor (BRF) of the land surface changes with the viewing and illumination geometries to decouple the atmospheric and surface scattering contributions with any accuracy. We note here that the BRF is defined as the ratio of surface-leaving radiance to the radiance from a Lambertian reflector under the same illumination conditions. North *et al.* [27] present a physical model of light scattering that can be used to retrieve land surface bidirectional reflectance and atmospheric aerosol

properties without recourse to *a priori* information of the land surface properties.

The ratio of surface directional reflectance at different viewing positions has shown to be approximately spectrally invariant in the optical bands of the ATSR-2 and AATSR [25], [26], [35], [36] and MISR instruments [37]. This is because the scattering elements of the surface are much larger than light at optical wavelengths; thus, the angular variation of surface reflectance is dominated by wavelength-independent geometric effects. The model-based retrieval approach of North *et al.* [27] is an extension of this assumption, taking into account the variation of diffuse light with wavelength. This is predicated on the theory that scattering by atmospheric aerosols increases the diffuse contribution of light at the surface. The anisotropy is reduced when the diffuse irradiance is high because the contrast between shadowed and sunlit surfaces decreases. Anisotropy is similarly dependent for bright targets, owing to the multiple scattering of light between the surface elements. The atmospheric scattering elements including aerosols and gas molecules are comparable in size to the wavelength of light at optical wavelengths. As a result, the effect of atmospheric scattering on the anisotropy will be a function of wavelength. Considering these contributions results in a physical model of spectral change with the viewing angle [27]

$$R_{\text{mod}}(\lambda, \Omega) = (1 - D(\lambda)) P(\Omega)w(\lambda) + \frac{\gamma w(\lambda)}{1 - g} [D(\lambda) + g(1 - D(\lambda))] \quad (1)$$

where  $g = (1 - \gamma)w(\lambda)$ ,  $\lambda$  is the wavelength,  $\Omega$  is the viewing geometry (forward or nadir view in the cases of ATSR-2 and AATSR),  $R_{\text{mod}}$  is the modeled BRDF,  $\gamma$  is the fraction contributing to higher order scattering,  $D$  is the fraction of diffuse irradiance,  $P$  is a structural parameter, and  $w$  is a spectral parameter. The first and second terms of (1) refer to direct and diffuse scattering, respectively.

Experiments with a large data set of natural surface reflectances performed in [27] have shown that a fixed value of 0.3 for  $\gamma$  can be used. The model separates the angular effects of the surface into two components, namely: 1) a structural parameter  $P$  that is dependent only on the view direction and 2) the spectral parameter  $w$  that is dependent only on the wavelength.  $P(\Omega)$  and  $w(\lambda)$  are free parameters that are retrieved. By inversion, this model of surface scattering has been shown theoretically to lead to a tractable inversion method, which is potentially more robust than the simple assumption of angular invariance alone [27] and which may be applied arbitrary to spectral wavebands [38]. The model has been applied to ATSR-2 [33] and can be applied to any set of multiangle measurements.

This model of surface scattering does not fully reconstruct the BRDF, and the shape of the BRDF is not prescribed. Instead, the model is a parameterization of the BRDF that allows us retrieve surface reflectance at the two viewing positions for the four AATSR channels. Models of the BRDF are generally not invertible given only two directional observations. The angular reflectance of a wide variety of natural land surfaces has been shown to fit this simple model in sensitivity studies

[27]. In contrast, reflectance that is a mixture of atmospheric and surface scattering does not fit this model well. As a result, the model can be used to estimate the degree of atmospheric contamination for a particular set of reflectance measurements and to find the atmospheric parameters that allow retrieval of a realistic surface reflectance.

AATSR channel radiance is provided as TOA reflectance using onboard calibration. Our aim is to retrieve the parameters characterizing the atmospheric aerosol and ground reflectance from the cloud-free AATSR TOA reflectance data for the four visible and near-infrared (NIR) bands in both the nadir and forward views by using this model of surface scattering. This is achieved through inversion of the Second Simulation of the Satellite Signal in the Solar Spectrum (6S) radiative transfer model [39]. However, this inverse problem is underconstrained inasmuch as it has fewer measurements than output model parameters that need to be retrieved. To constrain the model so that AOD is the only unknown atmospheric parameter, assumptions must be made concerning the other aerosol optical properties, including phase function, single-scattering albedo, and scattering and extinction coefficients. In practice, a range of models representing generalized aerosol types are used to constrain the inverse problem [22].

The inversion is achieved through iteration of a two-stage numerical process [27], the schematic of which is presented in Fig. 1. The first stage is to retrieve a set of eight ground reflectance values and estimates of diffuse irradiance at the four wavelengths given an initial estimate of the atmospheric aerosol model and AOD at 550 nm by inversion of the 6S radiative transfer model. The best fit of the two structural parameters  $P(\text{nadir})$  and  $P(\text{forward})$  and four spectral parameters  $w(555)$ ,  $w(660)$ ,  $w(870)$ , and  $w(1610)$  to (1) are found by using the iterative minimization method of Powell [40]. The second stage uses Brent line minimization [40] to converge on the optimum value for AOD. For each iteration, each estimate of AOD results in a different set of surface reflectance values. The optimum value of AOD is the best fit of surface reflectances to (1) and is attained by minimizing the error function  $E_{\text{mod}}$

$$E_{\text{mod}} = \sum_{\Omega=1}^2 \sum_{\lambda=1}^4 [R_{\text{surf}}(\lambda, \Omega) - R_{\text{mod}}(\lambda, \Omega)]^2 \quad (2)$$

where  $R_{\text{mod}}$  is the surface reflectance estimated using (1) based on the best fit values of the parameters  $P$  and  $w$  and  $R_{\text{surf}}$  is the surface reflectance calculated using 6S given the TOA reflectance  $R_{\text{toa}}$  and the estimated atmospheric profile. Surface reflectance is related to the TOA reflectance by [39]

$$R_{\text{surf}}(\theta_s, \theta_v, \phi_s - \phi_v, \lambda) = \frac{R'_{\text{toa}}}{1 + R'_{\text{toa}}S} \quad (3)$$

where  $\theta_s$  is the solar zenith angle,  $\theta_v$  is the view zenith angle,  $\phi_s$  is the solar azimuth angle,  $\phi_v$  view azimuth angle,  $S$  is the atmospheric spherical albedo, and  $R'_{\text{toa}}$  is

$$R'_{\text{toa}} = \frac{R_{\text{toa}}(\theta_s, \theta_v, \phi_s - \phi_v, \lambda) - R_{\text{atm}}(\theta_s, \theta_v, \phi_s - \phi_v, \lambda)}{T(\theta_s)T(\theta_v)} \quad (4)$$

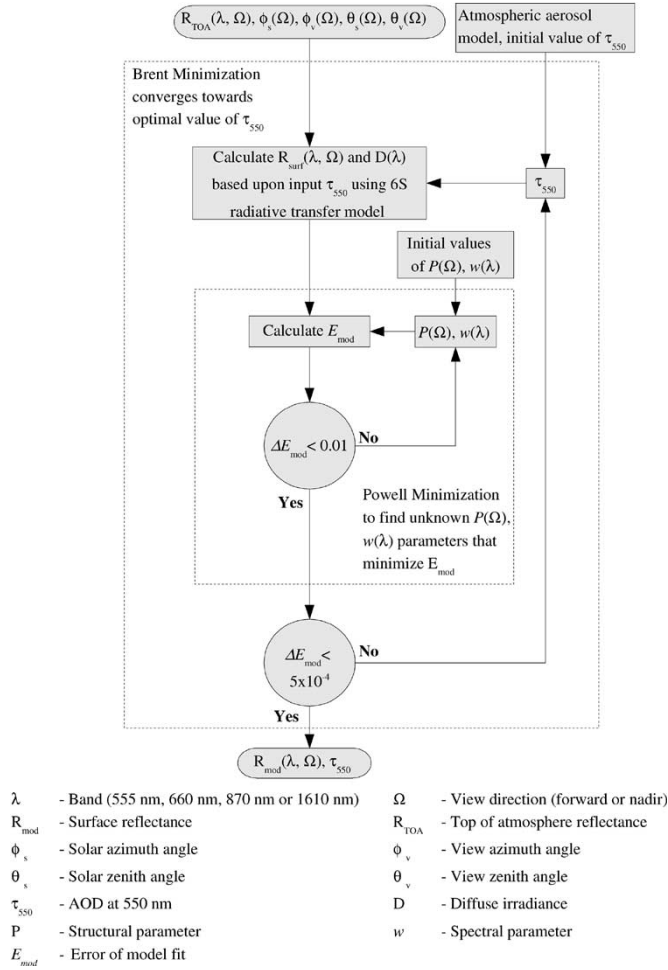


Fig. 1. Model inversion scheme to find the optimum AOD and land surface reflectance. This is achieved through iteration of a two-stage numerical process. The first stage uses Powell minimization to find the parameters  $P$  and  $w$  that minimizes  $E_{mod}$ . The second stage uses Brent line minimization to converge on the optimum value for AOD.

where  $R_{atm}$  is the intrinsic atmospheric reflectance and  $T(\theta_s)$  and  $T(\theta_v)$  denotes downward and upward transmittances, respectively.

The inversion procedure is applied to AATSR TOA reflectance. The derived parameters include a set of eight surface BRFs at four wavelengths and two angles, AOD at 550 nm and an estimate of the tropospheric aerosol model that falls into one of five compositional categories including continental (predominantly composed of dust-like particles), urban, maritime (sea salts), biomass (carbonaceous smoke particles), and desert dust. The optical properties of the continental, maritime, and urban models are calculated from a mixture of the basic components in Table I [39], [41], [42]. The biomass aerosol model is based on sun-photometer measurements taken in the Amazon [39], and the desert model assumes spherical particles and corresponds to background conditions described in [43]. We derive AOD at 550 nm because 6S parameterizes AOD by its value at 550 nm. AOD at other wavelengths are calculated according to the aerosol model determined during the inversion.

We do not prescribe the atmospheric aerosol model depending on location and time of year. Instead, the inversion is performed using each of the five atmospheric aerosol models

TABLE I  
BASIC AEROSOL COMPONENTS OF THE CONTINENTAL, MARITIME, AND URBAN AEROSOL MODELS WITH MIXING RATIOS

	Dust-like	Water soluble	Oceanic	Soot
Continental	0.70	0.29		0.01
Maritime		0.05	0.95	
Urban	0.17	0.61		0.22

separately and then selecting the candidate model on the basis of best fit by minimization of  $E_{mod}$ . The accuracy of the AOD estimates will depend on how well the aerosol model characterizes the atmospheric profile, and it assumes that the aerosol model that best characterizes the atmospheric profile will minimize  $E_{mod}$ . The flexibility in the selection of aerosol model allows us to take account of the spatial and temporal variability of aerosol microphysical characteristics.

### III. DATA

The model of surface scattering is applied to AATSR TOA reflectance data. A range of other data is also used in our analyses to allow for comparison and validation of the resulting AATSR aerosol and surface parameters, including Aerosol Robotic Network (AERONET)-derived aerosol properties, the TOMS AI, and the MODIS and MISR aerosol and surface products.

The surface scattering model is applied to cloud-free land surfaces within every AATSR image for which coincident sun-photometer measurements of AOD are available. Cloud-free AATSR image data for 19 test sites from around the world were acquired from ESA for the time period between July 2002 and March 2004. This comprises more than 200 level 1b gridded brightness temperature and reflectance (GBTR) images. Nominally, the AATSR instrument revisits the same area approximately once every six days at the equator, but the effective coverage is less because of clouds. In addition, 32 AATSR striplines covering the Sahel and southern Sahara region are acquired for March 2003 to produce a monthly composite of AOD.

The test sites were selected to coincide with the sites of permanent AERONET ground-based sun-photometer instruments [44]. AERONET is a global network of ground-based sun-photometers that measures solar and sky radiance from which AOD, single-scattering albedo, and particle-size distribution and other aerosol properties can be derived. These ground-based measurements were used for testing of the AATSR-derived estimates of AOD. The selected test sites represent a range of land surface types and aerosol sources between 53° N and 35° S (Fig. 2). In the majority of cases, the sun-photometer measurements were taken within approximately 1 h of the corresponding AATSR image acquisitions. Level 2 AERONET data that have been cloud-screened and quality-assured were used in the analysis [45]. To allow direct comparison with the satellite-derived aerosol estimates, the sun-photometer measurements were interpolated to 550 nm using

$$\tau_\lambda = \beta \lambda^\alpha \quad (5)$$

where  $\tau_\lambda$  is the AOD at wavelength  $\lambda$ ,  $\beta$  is the optical depth parameter, and  $\alpha$  is the Ångström exponent. The  $\beta$  and  $\alpha$

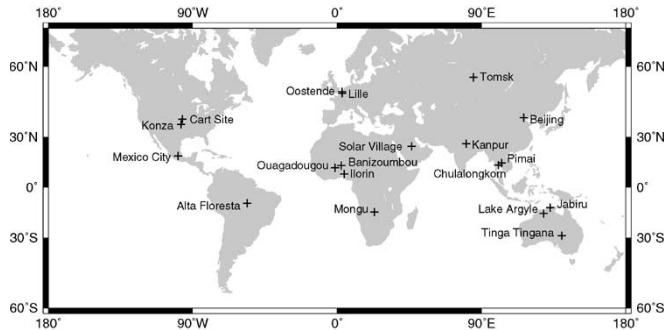


Fig. 2. World map of AERONET sites corresponding to acquired AATSR scenes. Over 200 images from 19 sites around the world at a range at latitudes and variety of land covers for different aerosol sources were acquired.

parameters were found by the least squares fit to the sun-photometer data in the spectral domain at wavelengths for which estimates of AOD were retrieved. The Ångström exponent is a measure of the dependence of AOD with wavelength and tends to decrease with particle size. For fine- (effective radius  $< 0.1 \mu\text{m}$ ) and accumulation-mode (effective radius  $> 0.1 \mu\text{m}$  and  $< 1 \mu\text{m}$ ) aerosol particles, such as those derived from biomass burning, the radiation at shorter wavelengths are more influenced by aerosol scattering than at longer wavelengths, and thus, the AOD is higher at shorter wavelengths. For coarse particles (effective radius  $> 1 \mu\text{m}$ ) including sea salts and desert dust that are typically larger than the wavelength of visible and NIR light, the Ångström exponent is small, and the AOD tends to be relatively constant at optical wavelengths.

For intersensor comparisons of aerosol products, global TOMS measurements of AI resampled to  $1.25^\circ \times 1^\circ$  from the Earth Probe satellite were also acquired. In addition, level 2 aerosol products of MODIS and MISR were acquired for a subset of these sites. For the daytime overpass, the Terra (platform of MODIS and MISR) and Envisat (platform of AATSR) satellites cross the equator at around 10:30 A.M. and 10:00 A.M. local time, respectively; therefore, the MODIS and MISR observations are almost coincident with the AATSR measurements. For the MISR product, measurements of AOD at 558 nm are provided with a sample spacing of 17.6 km every nine days at the equator [46], but at higher latitudes, the revisiting frequency is higher. The MODIS product provides daily coverage at a nominal spatial resolution of  $10 \times 10$  km using prescribed aerosol models over land [21], [47]. A range of aerosol parameters are retrieved including estimates of AOD at 550 nm.

The AATSR-derived estimates of surface reflectance are compared with the atmospherically corrected MOD43B1 MODIS BRDF/Albedo product and the BRDF parameters contained in the MISR level 2 surface reflectance product. MODIS images the Earth in 36 spectral bands and provides daily global coverage at high latitudes due to its wide swath width of 2300 km. Although MODIS only images the target from a single viewing position on each orbit, it is capable of acquiring measurements from different viewing positions for a target due to overlap between the images obtained on separate orbital overpasses over a period of a few days [48]. The MODIS BRDF/Albedo product is modeled from observations acquired

over a period of 16 days and sampled at a nominal 1 km. In contrast, MISR is capable of imaging the same point on the Earth's surface near simultaneously from nine different viewing positions in the along-track direction at four wavelengths centered at 446, 558, 672, and 866 nm. MISR is configured such that one radiometer points in the nadir direction and eight radiometers point at oblique angles relative to the Earth's surface both in the forward and aft directions with viewing angles of  $26.1^\circ$ ,  $45.6^\circ$ ,  $60.0^\circ$ , and  $70.5^\circ$  [49]. The MISR surface product contains a number of parameters sampled at 1.1 km, including the BRDF at the nine view directions and four wavelengths.

#### A. AATSR Preprocessing

Before applying the dual-view retrieval to the AATSR data, the data were preprocessed to remove artifacts that may cause the algorithm to fail. To reduce noise and minimize the effect of coregistration errors between the nadir and forward looks of the AATSR instrument, pixels within a  $15 \times 15$  km area of the location of the corresponding AERONET test site were averaged. In addition, the dual-angle retrieval approach is very sensitive to cloud-contaminated pixels. Therefore, a rigorous cloud mask is applied to each pixel within the  $15 \times 15$  km area to ensure that the algorithm is implemented only on cloud-free pixels. Pixels containing cloud were identified by applying a set of tests to the NIR and thermal channels as described in [50] and [51]. The resulting averaged pixel is only considered to be cloud-free if more than 40% of the pixels within the area are not identified as cloud. This is a rigorous cloud mask that occasionally causes more cloud obfuscation than necessary, particularly over bright surfaces with very high aerosol concentrations.

### IV. RESULTS AND DISCUSSION

#### A. Comparisons With Sun-Photometer Measurements

To test the accuracy of the AATSR-derived estimates of AOD at 550 nm, these measurements were compared with data acquired by the AERONET sun-photometers. Of the AATSR data that were acquired, there are 227 cloud-free coincident measurements of AOD between the AATSR and sun-photometers representing 19 sites around the world. These data are presented in Fig. 3, and a site-by-site summary of the statistics is given in Table II. There is close correlation between the sun-photometer and satellite-derived measurements of AOD. The overall Pearson's correlation coefficient  $r^2$  for all sites combined is 0.70, although the absolute error of the residuals increases with increasing AOD. The root-mean-square error (rmse) of all the data is 0.16, but when only values of aerosol opacity less than 0.5 (as measured by the sun-photometers) are considered, the rmse is reduced to 0.09. There is also little evidence of systematic error in the estimates of AOD as the mean AOD over all AERONET measurements is 0.27 compared with a mean of the AATSR-derived AOD estimates of 0.26.

Differences between the sun-photometer and AATSR-derived estimates of AOD may be due to a number of factors including the small time differences between acquisition of sun-photometer measurements and the satellite overpass,

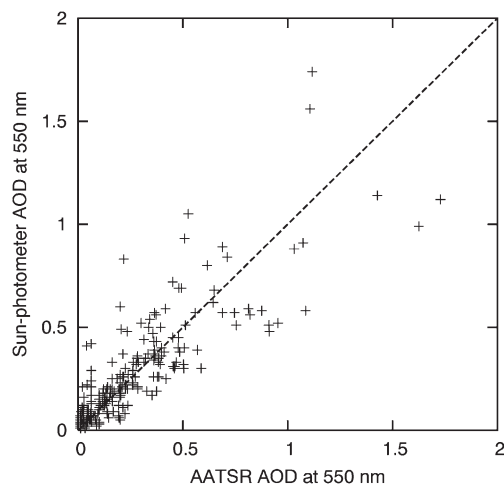


Fig. 3. Comparison of AATSR-derived estimates of aerosol optical thickness (AOT) at 550 nm with sun-photometer measurements for all sites. The dashed line represents the 1 : 1 line.

undetected subpixel cloud contamination, the selection of an aerosol model that does not properly characterize the atmospheric scattering, and heterogeneity of the land surface within the  $15 \times 15$  km area of AATSR observations. Occasionally, the inversion does fail, and this is possibly due to unrealistic characterization of atmospheric aerosols by the selected model. Failure to converge may be also due to an inappropriate model of surface scattering for some cases.

The performance of the retrieval algorithm differs across the sites. Table II shows that the Pearson's  $r^2$  between the AERONET- and AATSR-derived estimates of AOD vary widely from 0.39 at Mongu to 0.93 at Lille. The algorithm tends to perform best (i.e., where there is good agreement between the AERONET- and AATSR-derived estimates of AOD and residual error is low) over homogeneous vegetated areas with relatively low reflectances in the visible channels, such as Lille, Cart Site, Jabiru, and Konza. For these sites, the best fit aerosol model is biomass. The algorithm also performs well over heterogeneous semiarid land covers such as Ouagadougou in the Sahel. Moreover, accurate retrievals of AOD can be obtained over bright desert surfaces including Solar Village, Saudi Arabia. This is an important result because bright targets provide a robust test for the retrieval algorithm. For arid regions, the surface has high reflectance in the visible channels (0.37 at 660 nm); consequently, the relative contribution of atmospheric scattering to the top of atmosphere radiance is small, resulting in lower sensitivity to aerosols and potentially greater uncertainty in the derived estimates of AOD. Single-look sensors generally have difficulty in measuring aerosols over these land surfaces [20], but multilook sensors such as AATSR and MISR can retrieve AOD over bright surfaces [52]. Some sites typically have a low atmospheric aerosol content; hence, the signal is small relative to the residual error resulting in low  $r^2$ . However, the rmse is low for many of these sites; thus, the estimate is reliable.

To illustrate the capability of AATSR for routine monitoring of aerosols, a time series of AOD was retrieved for the Ouagadougou site in the West African Sahel over an 18-month period from August 2002 to January 2004 (Fig. 4).

Over this period, 25 cloud-free AATSR acquisitions were available; the remaining acquisitions were either contaminated by cloud or did not coincide with sun-photometer measurements. The AATSR and sun-photometer measurements are well correlated, where  $r^2 = 0.77$  on the basis of best fit for the aerosol model. The AOD tends to be high all year round with particularly high levels of AOD of greater than 1 during March 2003. It is possible to infer the type of aerosol from the AERONET retrievals of the Ångström exponent. At Ouagadougou, the Ångström exponent tends to be low (typically  $< 0.2$ ), indicating that the particles are large and spectrally neutral. This corresponds to the presence of dust throughout most of the year, including the AOD peak of March 2003. The primary aerosol type of this region is dust that has been transported from the Sahara Desert by the Harmattan winds. Between December and February, this region can also be affected by biomass-burning aerosols that have been produced from fires in the savanna vegetation. Smoke aerosols from biomass burning are small, typically of the order of a few tenths of microns, and have higher Ångström exponents [53].

The AATSR retrieval method was also developed to estimate other aerosol properties based on the best fit of a range of aerosol scattering models in the inversion procedure. For some of the sites, realistic parameters are obtained for a given land surface and likely aerosol source. These sites include: 1) Ilorin, which is located in the semiarid Sahelian zone and dominated by desert-dust aerosols; 2) Tomsk, which is located in the Siberian boreal forest and dominated by smoke aerosols from biomass burning; and 3) Jabiru, which is located on the Northern Australian coast and contains a mixture of biomass and maritime aerosols. However, this method does not reliably predict the correct aerosol model for the majority of sites.

At Ouagadougou, the desert-dust, biomass, and maritime aerosol models were selected on the basis of best fit for retrievals on individual dates. Although dust and biomass represent probable aerosol types, it is unlikely that sea-salt aerosols are present in significant quantities here. More likely is that the aerosol type has been incorrectly attributed to maritime instead of desert dust. Banizombou has a similar aerosol climatology to Ouagadougou, i.e., it is also influenced by desert dust, yet the dust aerosol model has not been selected on any date at this site. The industrialized areas of Beijing (China), Chulalongkorn (Bagnkok, Thailand), Kanpur (northern India), Lille (north-east France), Mexico City (Mexico), Oostende (Belgium), and Pimai (Thailand) are major sources of urban aerosols. However, the aerosol model that has been selected on the basis of best fit for these sites is biomass. It is evident that the model has difficulty discriminating urban from biomass aerosols, both of which tend to be composed of absorbing particles. Mongu, Zambia, is dominated by smoke from agricultural biomass burning [54], but there is also some windblown soil, which may account for the low Ångström exponent in some of the AERONET retrievals [53]. It is unlikely that maritime aerosols can ever be observed there. Alta Floresta, which is located in the Amazon, is also influenced by aerosols from biomass burning. Although the biomass aerosol model is selected by the retrieval algorithm for many cases, the maritime aerosol model is selected on some dates, which is clearly inappropriate for

TABLE II  
SUMMARY OF STATISTICS OF INTERCOMPARISONS BETWEEN AATSR AND SUN-PHOTOMETER ESTIMATES OF AOD.  
ITALICIZED  $r^2$  VALUES ARE STATISTICALLY SIGNIFICANT AT THE 95% CONFIDENCE LEVEL

Site	Land Cover	Time period	Number of samples	$r^2$	RMSE	Best-fit aerosol model	Mean $R_{surf}$ for forward view at 660 nm	Maximum AOD	Mean AOD
Alta Floresta, Brazil (-9.9°N, -56.0°E)	Primary forest, agriculture	12/08/02-26/09/03	11	<i>0.53</i>	0.22	Biomass & Maritime	0.08	1.13	0.41
Banizoumbou, Niger (13.5°N, 2.7°E)	Arid	18/10/02-17/09/03	14	<i>0.64</i>	0.27	Biomass & Maritime	0.27	1.12	0.58
Beijing, China (40.0°N, 116.4°E)	Urban	01/05/03-21/09/03	3	0.76	0.17	Biomass	0.10	0.69	0.47
Cart Site, US (36.6°N, -97.4°E)	Prairie, agriculture	09/05/03-09/03/04	11	<i>0.81</i>	0.04	Biomass	0.08	0.30	0.13
Chulalongkorn, Thailand (13.7°N, 100.5°E)	Urban, tropical	20/04/03-02/12/03	4	0.58	0.15	Biomass Continental	0.09	0.49	0.39
Ilorin, Nigeria (8.3°N, 4.3°E)	Urban, arid	24/12/02-09/01/03	3	0.97	0.14	Desert	0.08	0.89	0.71
Jabiru, Australia (-12.7°N, 132.9°E)	Sparse forest	24/03/03-01/10/03	11	<i>0.77</i>	0.05	Maritime & Biomass	0.09	0.37	0.14
Kanpur, India (26.5°N, 80.4°E)	Urban	23/03/03-07/03/04	14	<i>0.83</i>	0.21	Biomass	0.14	1.64	0.56
Konza, US (39.1°N, -96.6°E)	Prairie	25/09/02-27/12/03	20	<i>0.87</i>	0.04	Biomass	0.08	0.35	0.13
Lake Argyle, Australia (-16.1°N, 128.7°E)	Semi-arid rangeland	15/12/02-21/02/04	24	<i>0.43</i>	0.05	Maritime Biomass	0.14	0.28	0.08
Lille, France (50.6°N, 3.1°E)	Urban, agriculture	14/08/02-07/12/03	8	<i>0.90</i>	0.03	Biomass	0.08	0.32	0.15
Mexico City, Mexico (19.3°N, -99.2°E)	Urban	06/05/03-22/05/03	2			Biomass	0.12	0.58	0.55
Mongu, Zambia (-15.3°N, 23.2°E)	Savannah	02/12/02-04/11/03	19	<i>0.39</i>	0.17	Des., Bio. & Mar.	0.10	0.82	0.24
Oostende, Belgium (51.2°N, 2.9°E)	Urban, agriculture	14/08/02-22/09/03	7	0.59	0.08	Biomass	0.07	0.43	0.24
Ouagadougou, Burkina Faso (12.2°N, -1.4°E)	Semi-arid, Tropical	31/08/02-28/01/04	25	<i>0.77</i>	0.17	Des., Bio. & Mar.	0.19	1.74	0.44
Phimai, Thailand (15.2°N, 102.6°E)	Urban, tropical	11/04/03-31/12/03	4	0.46	0.16	Biomass	0.11	0.79	0.42
Solar Village, Saudi Arabia (24.9°N, 46.4°E)	Arid	04/10/02-09/03/04	29	<i>0.93</i>	0.22	Desert & Maritime	0.37	0.98	0.25
Tinga Tingana, Australia (-29.0°N, 140.0°E)	Arid	14/12/02-26/09/03	14	0.59	0.05	Maritime & Urban	0.36	0.22	0.09
Tomsk, Russia (56.5°N, 85.0°E)	Boreal forest	15/05/03-28/08/03	4	0.74	0.08	Biomass	0.06	0.36	0.22
All sites		31/08/02-09/03/04	227	<i>0.70</i>	0.16			1.64	0.27

this site. The maritime aerosol model is also selected on many occasions at the desert sites Tinga Tingana, Solar Village, and Lake Argyle, whereas on other occasions, the more appropriate desert-dust model is selected. The Southern Great Plains Cart Site and Konza Prairie are characterized by low AOD with clean continental aerosols; nevertheless, the biomass-burning aerosol model is selected in all cases. Occasionally, smoke from burning of vegetation is present.

The AATSR retrieval method has difficulty identifying the most appropriate aerosol type. The main problem is that the aerosol models are too generalized and more site-specific models are required. In particular, the nonspherical scattering of the dust particles is not considered in our AATSR retrievals. Models that take into account the nonsphericity of the dust particles more accurately predict the optical properties, but this is difficult to incorporate in remote sensing retrievals [55]. As a result of the inaccurate representation of the desert-dust aerosol model, the algorithm may choose a different aerosol model. Studies have shown that nonsphericity can be artificially simulated by a high concentration of fine particles [55], [56] and by strong absorption [57]. These two factors

could force the algorithm to choose strongly absorbing fine- and accumulation-mode biomass aerosols instead of nonabsorbing coarse dust particles. The problem is also recognized in the MISR [58], MODIS [21], and TOMS [59] retrievals of aerosol properties.

Retrievals of AOD at Ouagadougou were also performed by preselecting the desert-dust aerosol model (see Fig. 4). These estimates of AOD compare well with the AOD estimates based on the best fit aerosol model. However, prescribing the most appropriate aerosol model does not always result in improved estimates of AOD. This is because the algorithm is relatively insensitive to aerosol type in many cases [33]. In other situations, the accuracy of the AOD estimates can be reduced because we are constraining the retrieval to an imposed aerosol type that may be a poorer representation of the atmospheric profiles than the model chosen by best fit.

### B. Intersensor Comparisons of AOD

Intersensor comparisons with the estimates of AOD derived from the MISR and MODIS instruments and with the TOMS

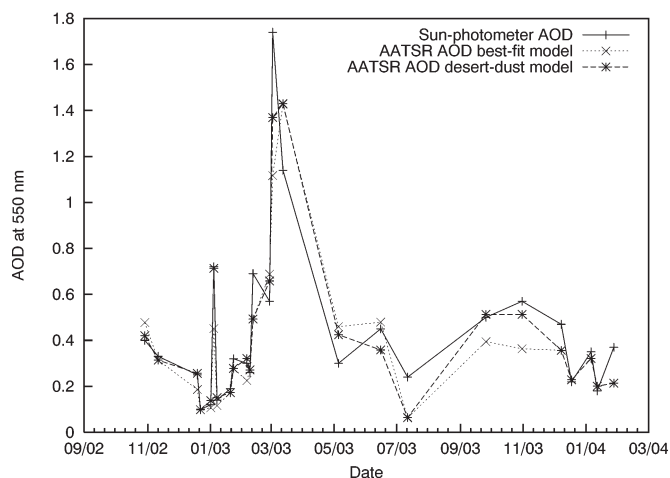


Fig. 4. Time series of AOD for the Ouagadougou site in the West African Sahel over an 18-month period from August 2002 to January 2004. The AATSR-derived estimates of AOD calculated using both the best fit and prescribed desert-dust aerosol models and the corresponding sun-photometer measurements are presented. The AATSR and sun-photometer measurements are well correlated ( $r^2 = 0.77$  for the best fit model) and show a peak of AOD during March 2003 due to desert dust.

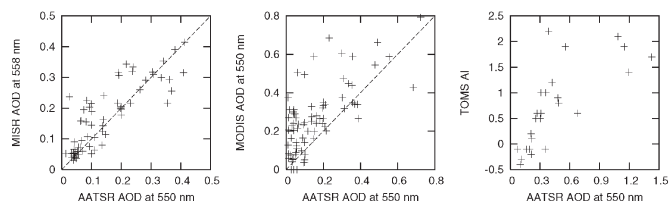


Fig. 5. Intersensor comparisons of AATSR estimates of AOT with MODIS (for Alta Floresta, Cart Site, Ilorin, Jabiru, Konza, Ouagadougou, Lille, Oostende, Lake Argyle, and Mongu sites) and MISR (for Cart Site, Jabiru, Konza, Lille, Mongu, Oostende, Ouagadougou, and Solar Village sites) measurements of AOD and TOMS AI (for Ouagadougou only). There is a systematic bias in the MODIS retrievals of AOD. The dashed line represents the 1 : 1 line.

AI product are performed as an additional means of cross-validation. The results of the intersensor comparisons are presented in Fig. 5 and Table III. The AATSR- and MISR-derived AODs show a high degree of correlation, where  $r^2 = 0.84$  for the eight sites for which coincident observations of AOD were acquired. There is high correlation between the two instruments' estimates of AOD for almost all the sites except Mongu, where some of the AATSR estimates of AOD are known to be inaccurate given their low correlation with the AERONET estimates, and Jabiru, where the residual error is low.

The overall correlation between the AATSR- and MODIS-derived estimates of AOD are lower ( $r^2 = 0.48$ ), although at some sites, there is good agreement between the two instruments' estimates of AOD. There is also systematic deviation between the AATSR and the MODIS retrievals. Mean AOD over all MODIS measurements is 0.28 compared with a mean of the AATSR-derived AOD estimates of 0.16. Given that there is little bias between the AERONET, AATSR, and MISR estimates and AOD, then the systematic error is due to MODIS overestimation of AOD at these sites. A similar bias has also been observed by Abdou *et al.* [60] and Chu *et al.* [61] during their evaluations of the MODIS aerosol product over land.

The overall correlation between AATSR AOD and the TOMS AI is poorer than for comparisons with MODIS and MISR ( $r^2 = 0.38$ ). This is because the AI is a function of several other factors such as the height of the aerosol layer and single-scattering albedo in addition to the AOD. In addition, TOMS is not sensitive to low-altitude aerosols [18].

### C. Surface Reflectance and Intersensor Comparisons

The technique is used to correct remotely sensed data for atmospheric scattering effects and to retrieve bidirectional surface reflectance. Bidirectional reflectance is calculated from TOA reflectance on basis of the AATSR-derived estimates of AOD and the best fit aerosol model for all sites. The surface reflectance may be increased or decreased when compared to the TOA reflectance, as in the case of the 550-nm channel (see Fig. 6). This is because of differences in the satellite and solar geometries, the albedo of the surface, and the scattering and absorbing properties of the atmosphere [62].

The sensitivity of the AATSR-derived surface reflectance to differences in estimates of AOD was also examined. Surface reflectance calculated based on the AATSR-derived estimates of AOD were compared with: 1) surface reflectance calculated using sun-photometer estimates of AOD and 2) surface reflectance calculated based on the atmospheric correction of Rayleigh scattering and gaseous absorption only, i.e., scattering and absorption of aerosols were not corrected for. Results show that there is very little difference in the surface reflectance calculated by implementing the inversion using either sun-photometer or AATSR-derived estimates of AOD (see Table IV). The rmse between bidirectional reflectance calculated using the different estimates of AOD is less than 0.01 for the infrared channels. The visible bands are more sensitive to differences in the estimates of AOD particularly in the forward view direction, owing to longer atmospheric path, and at 550 nm, due to greater scattering.

The uncertainty in the AATSR-derived estimates of surface reflectance are compared with retrievals from the MODIS BRDF/Albedo product and the MISR BRDF. We have selected images from multiple dates within 2002 and 2003 for a subset of the sites to incorporate surfaces with a range of reflectances in the analysis. These sites include Ouagadougou, Solar Village, Cart Site, Konza, Mongu, and Lille. Although MODIS images the Earth's surface in 36 spectral bands, only four of these wavebands corresponding to the AATSR channels shown in Table V are pertinent to this study. Likewise, only three of the four MISR and AATSR spectral channels allow for comparison.

AATSR, MODIS, and MISR have different angular sampling regimes, making direct comparisons between the BRDFs of the three instruments difficult given that the BRDFs vary according to the viewing and illumination geometries. The forward and nadir AATSR bidirectional surface reflectances are compared directly with the MISR surface reflectance for the 60° forward (Cf) and nadir (An) views, respectively. Although the MISR Cf and An views do not correspond exactly with the AATSR forward and nadir views, their geometries match closely given that the acquisitions are  $\sim 30$  min apart and the solar zenith angle is also similar. For the MODIS and AATSR comparisons,

TABLE III  
SUMMARY OF STATISTICS OF INTERSENSOR COMPARISONS OF AATSR ESTIMATES OF AOT WITH MODIS AND MISR MEASUREMENTS OF AOD AND TOMS AI. ITALICIZED  $r^2$  VALUES ARE STATISTICALLY SIGNIFICANT AT THE 95% CONFIDENCE LEVEL

Site	MISR			MODIS			TOMS		
	No. of samples	$r^2$	RMSE	No. of samples	$r^2$	RMSE	No. of samples	$r^2$	RMSE of AI
Alta Floresta				5	0.89	0.12	8	0.60	0.87
Banizoumbou							10	0.15	0.78
Beijing							3	0.01	1.15
Cart Site	3	0.99	0.01	6	0.89	0.08	9	0.50	1.14
Chulalongkorn							2		
Ilorin				1			1		
Jabiru	10	0.08	0.02	8	0.02	0.14	8	0.21	1.07
Kanpur							15	0.07	0.89
Konza	14	0.75	0.05	15	0.77	0.10	19	0.41	1.32
Lake Argyle				13	0.33	0.28	20	0.15	0.83
Lille	10	0.72	0.02	5	0.12	0.11	8	0.69	2.07
Mexico City							1		
Mongu	10	0.16	0.12	12	0.46	0.20	17	0.49	1.14
Oostende	1			3	0.84	0.14	7	0.01	1.48
Ouagadougou	16	0.89	0.11	9	0.69	0.12	25	0.55	0.63
Phimai							5	0.29	1.11
Solar Village	3	0.60	0.07				29	0.31	1.13
Tinga Tingana							9	0.15	0.83
Tomsk							2		
All sites combined	67	0.84	0.08	77	0.48	0.17	198	0.38	1.09

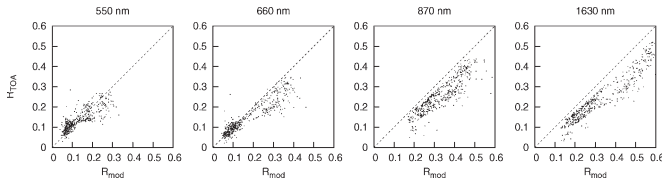


Fig. 6. Scatter plot of AATSR TOA reflectance versus bidirectional surface reflectance in nadir and forward views at all sites. The dashed line represents the 1 : 1 line.

TABLE IV  
SUMMARY OF STATISTICS OF COMPARISONS BETWEEN SURFACE REFLECTANCE CALCULATED USING THE ESTIMATES OF AOD DERIVED FROM AATSR AND SUN-PHOTOMETERS AND SURFACE REFLECTANCE CALCULATED WITHOUT CORRECTING FOR SCATTERING AND ABSORPTION OF AEROSOLS. THE  $r^2$  VALUES ARE SIGNIFICANT AT THE 99% CONFIDENCE LEVEL

Band (nm)	Nadir		Forward	
	$r^2$	RMSE	$r^2$	RMSE
AERONET $\tau_{550}$ versus AATSR $\tau_{550}$				
555	0.97	0.012	0.88	0.026
660	0.99	0.008	0.97	0.019
870	0.99	0.003	0.99	0.007
1610	0.99	0.002	0.99	0.005
AATSR $\tau_{550}$ versus $\tau_{550} = 0$				
555	0.91	0.025	0.69	0.055
660	0.98	0.017	0.92	0.041
870	0.99	0.007	0.98	0.015
1610	0.99	0.004	0.99	0.010

we use the MODIS BRDF/Albedo parameters to reconstruct the surface reflectance for the corresponding geometry of colocated AATSR observations.

A mathematical model of surface scattering can be used to describe the surface anisotropy [48]. The parameters that describe the BRDF shape are derived by inversion of a scattering model against angular observations of reflectance. Once these parameters are known, the bidirectional reflectance may be reconstructed for any viewing and solar positions by driving the model in the forward mode. In this way, MODIS retrieves the surface BRDF/Albedo parameters by fitting a three-parameter

TABLE V  
OVERLAP BETWEEN THE AATSR, MISR, AND MODIS SPECTRAL BANDS. NIR AND SWIR DENOTE NEAR AND SHORTWAVE INFRARED, RESPECTIVELY

	AATSR		MISR		MODIS	
	Band No.	Wavelength (nm)	Band No.	Wavelength (nm)	Band No.	Wavelength (nm)
Blue			1	423-458	3	459-479
Green	1	545-565	2	543-558	4	545-565
Red	2	647-669	3	663-678	1	620-670
NIR	3	855-875	4	853-878	2	841-876
SWIR	4	1580-1640			6	1628-1652

semiempirical kernel-driven BRDF model to a set of multiangle BRDF measurements [63]. MODIS is a single-look instrument, but the offset in the overlap between the Terra orbits allows the angular domain to be well sampled in the across-track direction. The BRDF model is the weighted sum of a constant isometric  $f_{iso}$  term and the volumetric  $f_{vol}$  and geometric  $f_{geo}$  Ross-Thick-Li-Sparse kernel-driven terms [48]

$$R_{surf}(\theta_v, \theta_s, \phi_v - \phi_s, \lambda) = f_{iso}(\lambda) + f_{vol}(\lambda)K_{vol} \times (\theta_v, \theta_s, \phi_v - \phi_s, \lambda) + f_{geo}(\lambda)K_{geo}(\theta_v, \theta_s, \phi_v - \phi_s, \lambda) \quad (6)$$

where  $K_{vol}$  and  $K_{geo}$  are the Ross-Thick and Li-Sparse kernels that describe the volumetric and geometric scatterings, respectively. Previous studies have shown that the Ross-Thick-Li-Sparse model is a good representation of the BRDF shape of natural surfaces [63]. The geometric, volumetric, and isotropic parameters are provided in the MODIS BRDF/Albedo product and allow reconstruction of reflectance for any viewing and illumination geometries.

The MISR BRF and MODIS bidirectional reflectances that have been reconstructed to the AATSR viewing and illumination geometries are compared with AATSR bidirectional reflectance for colocated observations on the corresponding dates. The mean bidirectional surface reflectance within a  $15 \times 15$  km area for a given site is calculated for all data sets to minimize pixel misregistration between the three data sets. The

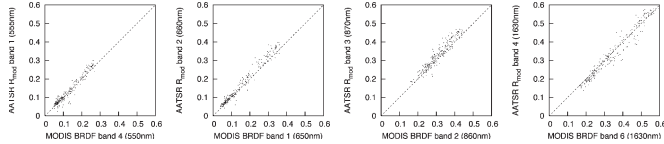


Fig. 7. Scatter plot of AATSR surface bidirectional surface reflectance in the nadir and forward views versus MODIS reflectance reconstructed at the corresponding AATSR viewing and illumination geometries for the Ouagadougou, Solar Village, Cart Site, Konza, Mongu, and Lille sites. The dashed line represents the 1 : 1 line, and the summary of statistics is presented in Table VI.

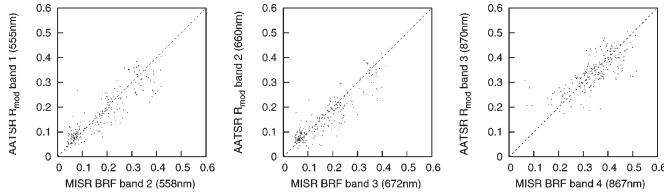


Fig. 8. Scatter plot of AATSR versus MISR surface bidirectional surface reflectance in the nadir and forward views at the Ouagadougou, Solar Village, Cart Site, Konza, Mongu, and Lille sites. The dashed line represents the 1 : 1 line, and the summary of statistics is presented in Table VI.

AATSR, MISR, and MODIS data sets used here are all sampled at approximately 1 km.

The AATSR, MISR, and MODIS estimates of bidirectional surface reflectance are in good agreement, as illustrated in Figs. 7 and 8 and Table VI. The scatter plots of the MODIS versus AATSR-derived estimates of bidirectional surface reflectance show that the residual errors are small and the points are located close to the 1 : 1 line for all spectral bands. The MODIS and AATSR estimates of bidirectional reflectance agree to an rmse of 0.03 or better. AATSR bands 1–3 slightly overestimate bidirectional reflectance when compared with MODIS, where the mean error is better than 0.02, whereas band 4 slightly underestimates reflectance. Agreement between AATSR and MISR is not as high as between AATSR and MODIS. This is most likely due to differences in angular sampling between the observations. In contrast with MODIS comparisons, AATSR-derived bidirectional reflectance tends to underestimate the BRF when compared with MISR at red wavelengths by about 0.01.

Differences between the AATSR, MISR, and MODIS estimates of bidirectional surface reflectance are due to a number of factors. First, the spectral bands and spectral response functions between the instruments do not match exactly (see Table V). Others have applied an empirical correction to account for this difference [64], but no such spectral adjustment is applied here. Second, there will be some geometric registration errors between the different instruments, although we have used the mean bidirectional surface reflectances over a small area. Third, the bidirectional surface reflectance from all three instruments have all undergone atmospheric correction with their own inherent uncertainties in their characterization of the atmospheric profile and aerosol retrieval. This is main source of error in the MISR surface retrievals [49]. Fourth, the MISR and AATSR bidirectional surface reflectance comparisons are acquired with slightly different illumination and viewing geometries. Fifth, there are errors associated with the fit of the MODIS

TABLE VI  
SUMMARY OF STATISTICS OF COMPARISONS BETWEEN AATSR AND MODIS AND MISR BIDIRECTIONAL SURFACE REFLECTANCE. WHEN ME IS NEGATIVE, AATSR ESTIMATES ARE LARGER THAN MISR AND MODIS AND VICE VERSA. THE  $r^2$  VALUES ARE SIGNIFICANT AT THE 99% CONFIDENCE LEVEL

Band number	Nadir		Forward				
	ME	$r^2$	ME	$r^2$			
AATSR	MODIS	ME	RMSE	ME	RMSE	$r^2$	
1	4	-0.01	0.02	0.96	0.00	0.02	0.93
2	1	-0.01	0.02	0.98	-0.01	0.03	0.97
3	2	-0.01	0.02	0.94	-0.02	0.03	0.89
4	6	0.00	0.02	0.97	0.01	0.03	0.94
MISR							
2	1	0.00	0.73	0.04	0.01	0.66	0.04
3	2	0.01	0.84	0.05	0.01	0.81	0.06
4	3	0.00	0.66	0.05	0.01	0.44	0.06

BRDF model to observed angular measurements of bidirectional surface reflectance. Finally, there may be some changes in the biophysical properties of the vegetated surfaces over the 16-day period for which the MODIS BRDF/Albedo is derived when compared with the AATSR-derived instantaneous surface reflectances. For the AATSR and MISR comparisons of surface reflectance, temporal differences in vegetation is not an issue because the data are acquired within  $\sim 30$  min of each other.

#### D. Regional-Scale Retrievals

The dual-angle retrieval method is applied on an image-basis to an entire  $500 \times 500$  km AATSR scene. To improve computational efficiency, precalculated lookup tables (LUTs) were created using the 6S radiative transfer model. The values within the LUTs are composed of the fraction of diffuse irradiance, incident surface radiance, atmospheric transmittance, and spherical albedo, allowing us to retrieve the aerosol properties and bidirectional surface reflectance. The parameters in the LUTs are dependent on the solar and viewing geometries and the atmospheric profile. The LUTs are constructed using 6S at the four visible and NIR bands of AATSR in four dimensions and indexed with AOD at 550 nm (from 0 to 3 at 0.05 intervals), solar zenith angle (from  $20^\circ$  to  $80^\circ$  at  $10^\circ$  intervals), view zenith angle (from  $0^\circ$  to  $60^\circ$  at  $10^\circ$  intervals), and relative azimuth angle  $|\phi_s - \phi_v|$  (from  $0^\circ$  to  $180^\circ$  at  $20^\circ$  intervals). The LUTs were generated for several candidate aerosol models.

During operation, values are estimated in the LUTs using multidimensional interpolation. By using LUTs, there will inevitably be a small decrease in the accuracy of the retrieved measurements compared with performing on-the-fly inversions, but the method gives an  $\sim 60$ -fold increase in speed [65]. To further improve efficiency, AOD is retrieved on a sparse grid (every ten pixels in the across-track direction and every ten pixels in along-track direction) across the scene, and values in between are spatially interpolated. Surface reflectance is calculated for every pixel. Given the atmospheric parameters contained in the LUTs, we can calculate the surface reflectance for the four AATSR channels at the two viewing positions using (3).

This LUT approach has previously been applied to dark vegetated surfaces [33]. Here, it is shown that image-based and regional-scale retrievals can be performed over heterogeneous land covers with high bidirectional reflectance. An AATSR

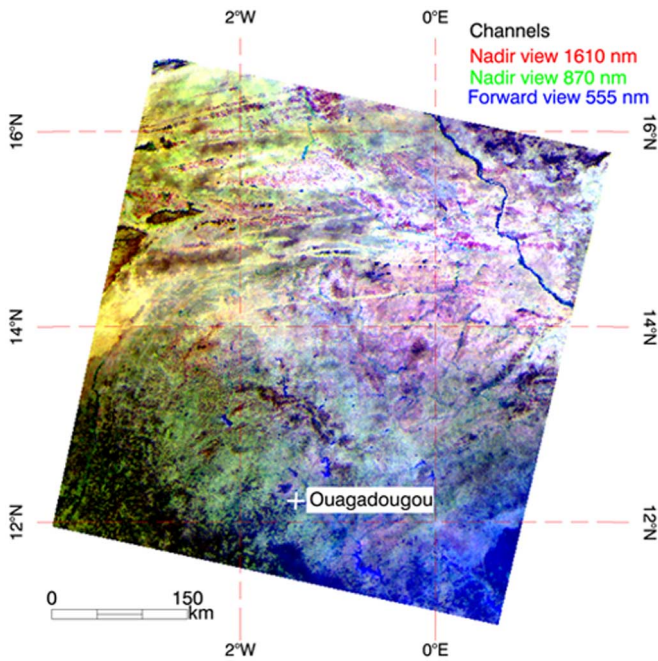


Fig. 9. TOA false color image acquired by AATSR over a region in the Sahel on January 5, 2003. The image covers an area of approximately 500 × 500 km. A smoke plume is visible in the southeast of the image.

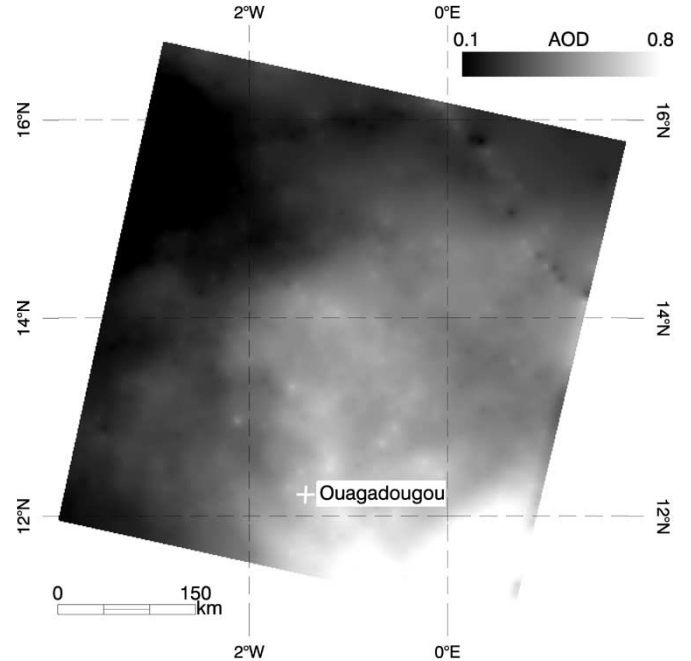


Fig. 11. Retrieved image of AOT at 555 nm. There is a high spatial variation, with AOD ranging from 0.1 to 0.8 within the 500 × 500 km region.

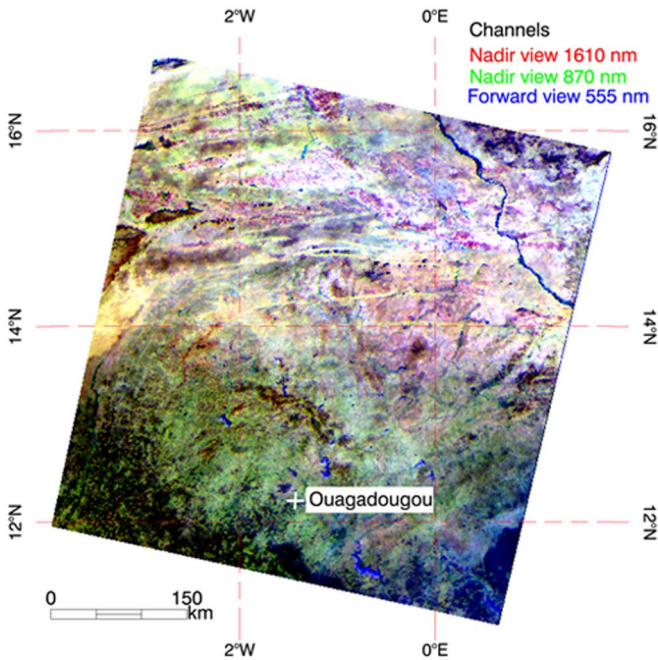


Fig. 10. AATSR image of surface reflectance after atmospheric correction.

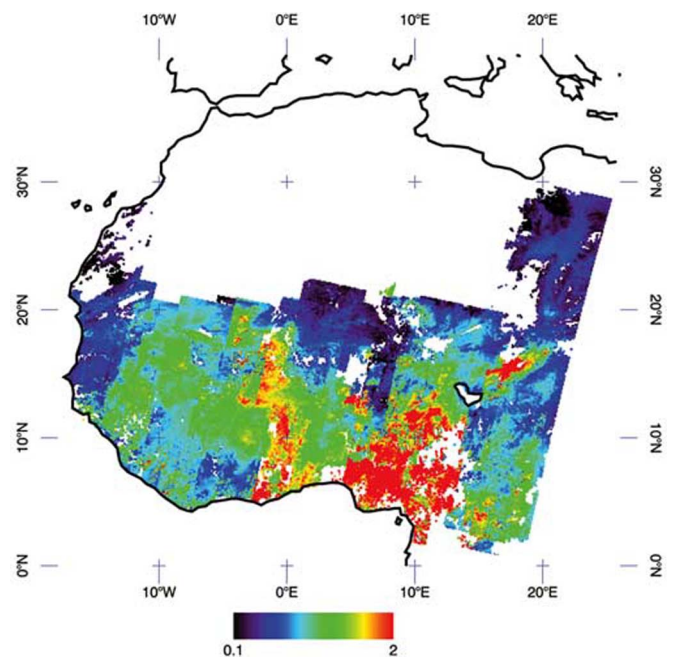


Fig. 12. Map of AATSR retrieved AOT at 555 nm of the Sahel and southern Sahara during March 2003. The mosaic is made up from thirty-two 500-km-wide AATSR striplines. AOD is higher (greater than 1.5) within Nigeria and Cameroon.

false color image of an area of the Sahel covering Burkina Faso, which includes the Ouagadougou site acquired on January 5, 2003, is shown in Fig. 9. The region contains semiarid and arid land cover in the north and subtropical land in the south. A large aerosol plume in the southeast of the image is clearly evident in the forward 555-nm channel. Here, the AOD is as high as 0.8. The result of the inversion is an image of bidirectional surface reflectance (Fig. 10) and a separate map of AOD (Fig. 11) that was produced using the biomass aerosol

model. The resulting bidirectional surface reflectance image contains very little scattering due to the atmosphere.

This image is mainly composed of desert dust and biomass aerosols. At the Ouagadougou AERONET site, the aerosol is predominantly composed of desert dust as inferred by the low Ångström values. However, the aerosol plume in the southeast portion of the image over the vegetated area has most likely been derived from anthropogenic biomass burning of vegetation in the Sahel. Between December and February of each year, the

savanna vegetation in the Sudanian zone is burned to clear the land for agricultural cultivation.

This approach is extended from image-based to regional-scale retrievals. Thirty-two relatively cloud-free AATSR striplines covering the Sahel and southern Sahara region are used to produce a monthly composite of AOD for March 2003 (Fig. 12). The inversion using the LUTs is implemented on each of the striplines. A spatially and temporally composited mosaic of the all striplines for AOD at 550 nm is presented in Fig. 12. The mosaic has a pixel size of 5 arc min (0.083°). AOD is calculated for each stripline, and then, the value of each pixel within the composite is calculated from the spatial and temporal mean of the nearest neighbours from each stripline. AOD cannot be retrieved for areas where no cloud-free data are available within the one-month period. Within Nigeria and Cameroon, there are high levels of AOD, owing to elevated levels of desert dust in the atmosphere.

The time taken to process an AATSR stripline will vary depending on the extent of cloud cover, the resolution at which the AOD estimates are retrieved and on the computer hardware. For instance, it took approximately 12 h to process the 32 AATSR striplines to produce the composite image of AOD in Fig. 12 at a pixel size of 5 arc min using a single prescribed aerosol model. The processing was performed on a personal computer with an Intel Xeon 2.8-GHz microprocessor and 1 GB of double data rate 266 memory. This demonstrates the capability of the LUT approach for retrieving AOD operationally at regional and global scales using relatively modest computational resources.

## V. CONCLUSION

AOD and bidirectional reflectance over land are derived using a physical model of light scattering that requires no *a priori* knowledge of the land surface. The algorithm applied to multiangle AATSR data was implemented for a number of sites around the world to test its operation over a range of land covers and aerosol types. Results show good agreement ( $r^2 = 0.70$  for all sites combined) between the AATSR-derived estimates of AOD and sun-photometer measurements. The retrieval performs best over vegetated land covers for biomass aerosol types. AOD can also be accurately retrieved over bright desert targets. Intersensor comparisons with the estimates of AOD derived from the MISR and MODIS instruments and with the TOMS AI product were also performed. There is high correlation between AATSR-derived AOD and MISR-derived aerosol estimates, where  $r^2 = 0.84$ , but the correlation of the AATSR-derived AOD with MODIS-derived AOD and TOMS AI is lower. Discrimination between aerosol types was tested but was found to be only partially successful.

Aerosol measurements can also be used for atmospheric correction of remotely sensed data, allowing surface reflectance to be compared over time. This is useful because AATSR and archived ATSR-2 data provide a long time series of global observations spanning more than a decade. The AATSR-derived surface reflectances were compared with the MODIS BRDF/Albedo and MISR surface products and were shown to correspond with rmse of 0.03 and 0.06 or better, respectively. A map of AOD covering the Sahel and southern Sahara region

was produced to demonstrate that AOD and surface reflectance can be retrieved at regional and potentially global scales.

## ACKNOWLEDGMENT

The authors thank the European Space Agency for providing the AATSR data through the Announcement of Opportunity for Envisat; the AERONET principal investigators, including D. Tanré and B. Holben, and their staff for establishing and maintaining the AERONET sites used in this investigation; the National Aeronautics and Space Administration (NASA) Distributed Active Archive Center for providing the MODIS and MISR aerosol and surface products; and the NASA Goddard Space Flight Center for providing the TOMS data.

## REFERENCES

- [1] C. Tucker, D. Slayback, J. Pinzon, S. Los, R. Myneni, and M. Taylor, "Higher northern latitude normalized difference vegetation index and growing season trends from 1982 to 1999," *Int. J. Biometeorol.*, vol. 45, no. 4, pp. 184–190, Nov. 2001.
- [2] R. Myneni, S. Maggion, J. Jaquinto, J. Privette, N. Gobron, B. Pinty, D. Kimes, M. Verstraete, and D. Williams, "Optical remote-sensing of vegetation—Modeling, caveats, and algorithms," *Remote Sens. Environ.*, vol. 51, no. 1, pp. 169–188, 1995.
- [3] S. Los, G. Collatz, P. Sellers, C. Malmstrom, N. Pollack, R. DeFries, L. Bounoua, M. Parris, C. Tucker, and D. Dazlich, "A global 9-yr biophysical land surface dataset from NOAA AVHRR data," *J. Hydrometeorol.*, vol. 1, no. 2, pp. 183–199, Apr. 2000.
- [4] P. North, "Estimation of fAPAR, LAI and vegetation fractional cover from ATSR-2 imagery," *Remote Sens. Environ.*, vol. 80, no. 1, pp. 114–121, 2002.
- [5] M. King, Y. Kaufman, D. Tanré, and T. Nakajima, "Remote sensing of tropospheric aerosols from space: Past, present, and future," *Bull. Amer. Meteorol. Soc.*, vol. 80, no. 11, pp. 2229–2259, 1999.
- [6] R. Charlson, S. Schwartz, J. Hales, R. Cess, J. Coakley, J. Hansen, and D. Hofmann, "Climate forcing by anthropogenic aerosols," *Science*, vol. 255, no. 5043, pp. 423–430, Jan. 1992.
- [7] M. Andreae, C. Jones, and P. Cox, "Strong present-day aerosol cooling implies a hot future," *Nature*, vol. 435, no. 30, pp. 1187–1190, Jun. 2005.
- [8] J. Kiehl and B. Briegleb, "The relative roles of sulfate aerosols and greenhouse gases in climate forcing," *Science*, vol. 260, no. 5106, pp. 311–314, Apr. 1993.
- [9] N. Bellouin, O. Boucher, J. Haywood, and M. Reddy, "Global estimation of aerosol direct radiative forcing from satellite measurements," *Science*, vol. 438, no. 7071, pp. 1138–1141, Dec. 2005.
- [10] L. Gu, D. Baldocchi, S. Wofsy, J. Munger, J. Michalsky, S. Urbanski, and T. Boden, "Response of a deciduous forest to the Mount Pinatubo eruption: Enhanced photosynthesis," *Science*, vol. 299, no. 5615, pp. 2035–2038, Mar. 2003.
- [11] P. Alton, P. North, J. Kaduk, and S. Los, "Radiative transfer modeling of direct and diffuse sunlight in a Siberian pine forest," *J. Geophys. Res.*, vol. 110, no. D23209, Dec. 2005. DOI: 10.1029/2005JD006060.
- [12] J. Hansen and A. Lacis, "Sun and dust versus greenhouse gases: An assessment of their relative roles in global climate change," *Nature*, vol. 346, no. 6286, pp. 713–719, Aug. 1990.
- [13] J. Houghton, Y. Ding, D. Griggs, M. Noguier, P. van der Linden, and D. Xiaosu, Eds. *Climate Change 2001: The Scientific Basis*, Cambridge, U.K.: Cambridge Univ. Press, 2001.
- [14] Y. Kaufman, D. Tanré, and O. Boucher, "A satellite view of aerosols in the climate system," *Nature*, vol. 419, no. 6903, pp. 215–223, Sep. 2002.
- [15] C. Rao, L. Stowe, and E. McClain, "Remote-sensing of aerosols over the oceans using AVHRR data theory, practice and applications," *Int. J. Remote Sens.*, vol. 10, no. 4, pp. 743–749, 1989.
- [16] L. Stowe, A. Ignatov, and R. Singh, "Development, validation, and potential enhancements to the second-generation operational aerosol product at the national environmental satellite, data, and information service of the national oceanic and atmospheric administration," *J. Geophys. Res.—Atmos.*, vol. 102, no. D14, pp. 16 923–16 934, 1997.
- [17] B. Holben, E. Vermote, Y. Kaufman, D. Tanré, and V. Kalb, "Aerosol retrieval over land from AVHRR data—Application for atmospheric correction," *IEEE Trans. Geosci. Remote Sens.*, vol. 30, no. 2, pp. 212–222, Mar. 1992.

- [18] N. Hsu, J. Herman, O. Torres, B. Holben, D. Tanré, T. Eck, A. Smirnov, B. Chatenet, and F. Lavenu, "Comparisons of the TOMS aerosol optical thickness: Results and applications," *J. Geophys. Res.*, vol. 104, no. D6, pp. 6269–6279, 1999.
- [19] O. Torres, J. Herman, P. Bhartia, A. Sinyuk, P. Ginoux, and B. Holben, "A long-term record of aerosol optical depth from TOMS observations and comparison to AERONET measurements," *J. Atmos. Sci.*, vol. 59, no. 3, pp. 398–413, 2002.
- [20] Y. Kaufman, A. Wald, L. Remer, B.-C. Gao, R.-R. Li, and L. Flynn, "The MODIS 2.1- $\mu\text{m}$  channel—Correlation with visible reflectance for use in remote sensing of aerosol," *IEEE Trans. Geosci. Remote Sens.*, vol. 35, no. 5, pp. 1286–1298, Sep. 1997.
- [21] L. A. Remer, Y. J. Kaufman, D. Tanré, S. Mattoo, D. A. Chu, J. V. Martins, R.-R. Li, C. Ichoku, R. C. Levy, R. Kleidman, T. F. Eck, E. Vermote, and B. N. Holben, "The MODIS aerosol algorithm, products and validation," *J. Atmos. Sci.*, vol. 62, no. 4, pp. 947–973, Apr. 2005.
- [22] J. Martonchik, D. Diner, R. Kahn, T. Ackerman, M. Verstraete, B. Pinty, and H. Gordon, "Techniques for the retrieval of aerosol properties over land and ocean using multiangle imaging," *IEEE Trans. Geosci. Remote Sens.*, vol. 36, no. 4, pp. 1212–1227, Jul. 1998.
- [23] J. Martonchik, D. Diner, K. Crean, and M. Bull, "Regional aerosol retrieval results from MISR," *IEEE Trans. Geosci. Remote Sens.*, vol. 40, no. 7, pp. 1520–1531, Jul. 2002.
- [24] J.-L. Roujean, D. Tanré, F.-M. Brecon, and J.-L. Deuze, "Retrieval of land surface parameters from airborne POLDER bidirectional reflectance distribution function during HAPEX-Sahel," *J. Geophys. Res.*, vol. 102, no. D10, pp. 11201–11218, 1997.
- [25] R. Flowerdew and J. Haigh, "Retrieval of aerosol optical thickness over land using the ATSR-2 dual-look satellite radiometer," *Geophys. Res. Lett.*, vol. 24, no. 4, pp. 351–354, 1996.
- [26] J. Veefkind, G. de Leeuw, and P. Durkee, "Retrieval of aerosol optical depth over land using two-angle view satellite radiometry during TARFOX," *Geophys. Res. Lett.*, vol. 25, no. 16, pp. 3135–3138, 1998.
- [27] P. North, S. Briggs, S. Plummer, and J. Settle, "Retrieval of land surface bidirectional reflectance and aerosol opacity from ATSR-2 multi-angle imagery," *IEEE Trans. Geosci. Remote Sens.*, vol. 37, no. 1, pp. 526–537, Jan. 1999.
- [28] C. Godslave, "Simulation of ATSR-2 optical data and estimates of land surface reflectance using simple atmospheric corrections," *IEEE Trans. Geosci. Remote Sens.*, vol. 34, no. 5, pp. 1204–1212, Sep. 1996.
- [29] D. Llewellyn-Jones, M. Edwards, C. Mutlow, A. Birks, I. Barton, and H. Tait, "AATSR: Global-change and surface-temperature measurements from Envisat," *ESA Bull.*, vol. 105, pp. 11–21, Feb. 2001.
- [30] M. Leroy and J.-L. Roujean, "Sun and view angle corrections on reflectances derived from NOAA/AVHRR data," *IEEE Trans. Geosci. Remote Sens.*, vol. 32, no. 3, pp. 684–697, May 1994.
- [31] M. Barnsley, P. Lewis, M. Sutherland, and J.-P. Muller, "Estimating land surface albedo in the HAPEX-Sahel southern super-site: Inversion of two BRDF models against multiple angle ASAS images," *J. Hydrol.*, vol. 188–189, no. 1–4, pp. 749–778, Feb. 1997.
- [32] J. Qi, F. Cabot, M. Moran, and G. Dedieu, "Biophysical parameter estimations using multidirectional spectral measurements," *Remote Sens. Environ.*, vol. 54, no. 1, pp. 71–83, Oct. 1995.
- [33] P. North, "Estimation of aerosol opacity and land surface bidirectional reflectance from ATSR-2 dual-angle imagery: Operational method and validation," *J. Geophys. Res.*, vol. 107, no. D12, 2002. DOI: 10.1029/2000JD000207.
- [34] C. Gonzalez, J. Veefkind, and G. de Leeuw, "Aerosol optical depth over Europe in August 1997 derived from ATSR-2 data," *Geophys. Res. Lett.*, vol. 27, no. 7, pp. 955–958, Apr. 2000.
- [35] J. Veefkind, G. de Leeuw, P. Stammes, and R. Koelemeijer, "Regional distribution of aerosol over land, derived from ATSR-2 and GOME," *Remote Sens. Environ.*, vol. 74, no. 3, pp. 377–386, 2000.
- [36] G. Mackay, M. Steven, and J. Clark, "An atmospheric correction procedure for the ATSR-2 visible and near-infrared land surface data," *Int. J. Remote Sens.*, vol. 19, no. 15, pp. 2949–2968, Oct. 1998.
- [37] D. Diner, J. Martonchik, R. Kahn, B. Pinty, N. Gobron, D. Nelson, and B. Holben, "Using angular and spectral shape similarity constraints to improve MISR aerosol and surface retrievals over land," *Remote Sens. Environ.*, vol. 94, no. 2, pp. 155–171, 2005.
- [38] J. Settle, "On the dimensionality of multi-view hyperspectral measurements of vegetation," *Remote Sens. Environ.*, vol. 90, no. 2, pp. 235–242, Mar. 2004.
- [39] E. Vermote, D. Tanré, J. Deuze, M. Herman, and J.-J. Morcette, "Second simulation of the satellite signal in the solar spectrum, 6S: An overview," *IEEE Trans. Geosci. Remote Sens.*, vol. 35, no. 3, pp. 675–686, May 1997.
- [40] W. Press, S. Teukolsky, W. Vetterling, and B. Flannery, *Numerical Recipes in C, The Art of Scientific Computing*, 2nd ed. Cambridge, U.K.: Cambridge Univ. Press, 1992.
- [41] G. d'Almeida, P. Koepke, and E. Shettle, *Atmospheric Aerosols: Global Climatology and Radiative Characteristics*. Hampton, VA: A. Deepak, 1991.
- [42] *Radiation Commission of IAMAP Meeting of Experts on Aerosols and Their Climatic Effect*, Mar. 1983, Williamsburg, VA: World Meteorol. Org.
- [43] E. Shettle, "Optical and radiative properties of a desert aerosol model," in *Proc. Symp. Radiation Atmosphere*, 1984, pp. 74–77.
- [44] B. Holben, Y. Kaufman, T. Eck, I. Slutsker, and D. Tanré, "AERONET—A federated instrument network and data archive for aerosol characterization," *Remote Sens. Environ.*, vol. 66, no. 1, pp. 1–16, 1998.
- [45] A. Smirnov, B. Holben, T. Eck, O. Dubovik, and I. Slutsker, "Cloud-screening and quality control algorithms for the AERONET database," *Remote Sens. Environ.*, vol. 73, no. 3, pp. 337–349, 2000.
- [46] D. Diner, W. Abdou, T. Ackerman, K. Crean, H. Gordon, R. Kahn, J. Martonchik, S. McMuldroy, S. Paradise, B. Pinty, M. Verstraete, M. Wang, and R. West, *MISR level 2 aerosol retrieval algorithm theoretical basis document*, 2001. Tech. Rep. Pasadena, CA: Jet Propulsion Lab. [Online]. Available: [http://modis.gsfc.nasa.gov/data/atbd/land\\_atbd.php](http://modis.gsfc.nasa.gov/data/atbd/land_atbd.php)
- [47] Y. Kaufman and D. Tanré, *Algorithm for remote sensing of tropospheric aerosol from MODIS, algorithm theoretical basis document, ATBD-MOD-02*, 1998. Tech. Rep. Greenbelt, MD: NASA Goddard Space Flight Center. [Online]. Available: [http://modis.gsfc.nasa.gov/data/atbd/land\\_atbd.php](http://modis.gsfc.nasa.gov/data/atbd/land_atbd.php)
- [48] A. Strahler, W. Wanner, C. Schaaf, X. Li, B. Hu, J.-P. Muller, P. Lewis, and M. Barnsley, *MODIS BRDF/Albedo product: Algorithm theoretical basis document*, 1996. Tech. Rep. Boston, MA: Boston Univ. [Online]. Available: [http://modis.gsfc.nasa.gov/data/atbd/land\\_atbd.php](http://modis.gsfc.nasa.gov/data/atbd/land_atbd.php)
- [49] D. Diner, J. Beckert, T. Reilly, C. Bruegge, J. Conel, R. Kahn, J. Martonchik, T. Ackerman, R. Davies, S. Gerstel, H. Gordon, J.-P. Muller, R. Myneni, P. Sellers, B. Pinty, and M. Verstraete, "Multi-angle Imaging SpectroRadiometer (MISR) instrument description and experiment overview," *IEEE Trans. Geosci. Remote Sens.*, vol. 36, no. 4, pp. 1072–1087, Jul. 1998.
- [50] L. Stowe, E. McClain, R. Carey, P. Pellegrino, G. Gutman, P. Davis, C. Long, and S. Hart, "Global distribution of cloud cover derived from NOAA/AVHRR operational satellite data," *Adv. Space Res.*, vol. 11, no. 3, pp. 51–54, 1991.
- [51] A. Zavody, C. Mutlow, and D. Llewellyn-Jones, "Cloud clearing over the ocean in the processing of data from the Along-Track Scanning Radiometer (ATSR)," *J. Atmos. Ocean. Technol.*, vol. 17, no. 5, pp. 595–615, 2000.
- [52] J. Martonchik, D. Diner, R. Kahn, B. Gaitley, and B. Holben, "Comparison of MISR and AERONET aerosol optical depths over desert sites," *Geophys. Res. Lett.*, vol. 31, no. L16102, 2004.
- [53] B. Holben, D. Tanré, A. Smirnov, T. Eck, I. Slutsker, N. Abuhassan, W. Newcomb, J. Schafer, B. C. F. Lavenu, Y. J. Kaufman, J. Van de Castle, A. Setzer, B. Markham, D. Clark, R. Fouin, R. Halthore, A. Karneli, N. T. O'Neill, C. Pietras, R. Pinker, K. Voss, and G. Zibordia, "An emerging ground-based aerosol climatology: Aerosol optical depth from AERONET," *J. Geophys. Res.*, vol. 106, no. 12, pp. 12067–12097, 2001.
- [54] O. Dubovik, B. N. Holben, T. F. Eck, A. Smirnov, Y. Kaufman, M. King, D. Tanré, and I. Slutsker, "Variability of absorption and optical properties of key aerosol types observed in worldwide locations," *J. Atmos. Sci.*, vol. 59, no. 3, pp. 590–608, 2002.
- [55] O. Dubovik, A. Smirnov, B. Holben, M. King, Y. Kaufman, T. Eck, and I. Slutsker, "Accuracy assessments of aerosol optical properties retrieved from AERONET sun and sky radiance measurements," *J. Geophys. Res.*, vol. 105, no. D8, pp. 9791–9806, 2000.
- [56] O. Dubovik, B. N. Holben, T. Lapyonok, A. Sinyuk, M. I. Mishchenko, P. Yang, and I. Slutsker, "Non-spherical aerosol retrieval method employing light scattering by spheroids," *Geophys. Res. Lett.*, vol. 29, no. 10, 2002.
- [57] H. Volten, O. Munoz, E. Rol, J. F. de Haan, W. Vassen, J. W. Hovenier, K. Muinonen, and T. Nousiainen, "Scattering matrices of mineral aerosol particles at 441.6 nm and 632.8 nm," *J. Geophys. Res.*, vol. 106, no. D15, pp. 17 375–17 401, 2001.
- [58] R. Kahn, R. West, and D. McDonald, "Sensitivity of multiangle remote sensing observations to aerosol sphericity," *J. Geophys. Res.*, vol. 102, no. D14, pp. 16 861–16 870, 1997.

- [59] A. Sinyuk, O. Torres, and O. Dubovik, "Combined use of satellite and surface observations to infer the imaginary part of refractive index of Saharan dust," *Geophys. Res. Lett.*, vol. 30, no. 2, 2003.
- [60] W. Abdou, D. Diner, J. Martonchik, C. Bruegge, R. Kahn, B. Gaitley, K. Crean, L. Remer, and B. Holben, "Comparison of coincident Multi-angle Imaging Spectroradiometer and Moderate Resolution Imaging Spectroradiometer aerosol optical depths over land and ocean scenes containing aerosol robotic network sites," *J. Geophys. Res.*, vol. 110, no. D10S07, 2005.
- [61] D. Chu, Y. Kaufman, C. Ichoku, L. Remer, Tanré and B. Holben, "Validation of MODIS aerosol optical depth retrieval over land," *Geophys. Res. Lett.*, vol. 29, no. 2, 2002.
- [62] H. Rahman and G. Dedieu, "SMAC: A simplified method for the atmospheric correction of satellite measurements," *Int. J. Remote Sens.*, vol. 15, no. 1, pp. 123–143, 1994.
- [63] C. Schaaf, G. Feng, A. Strahler, W. Lucht, X. Li, T. Tsang, N. Strugnell, X. Zhang, Y. Jin, J.-P. Müller, P. Lewis, M. Barnsley, P. Hobson, M. Disney, G. Roberts, M. Dunderdale, C. Doll, R. d'Entremont, B. Hu, S. Liang, J. Privette, and D. Roy, "First operational BRDF, albedo nadir reflectance products from MODIS," *Remote Sens. Environ.*, vol. 83, no. 1/2, pp. 135–148, Nov. 2002.
- [64] H. Fang, S. Liang, M. Chen, C. Walthall, and C. Daughtry, "Statistical comparison of MISR, ETM+ and MODIS land surface reflectance and albedo products of the BARC land validation core site, USA," *Int. J. Remote Sens.*, vol. 25, no. 2, pp. 409–422, 2004.
- [65] W. Grey, P. North, and S. Los, "Computationally efficient method for retrieving aerosol optical depth from ATSR-2 and AATSR data," *Appl. Opt.*, vol. 45, no. 12, pp. 2786–2795, 2006.



**Peter R. J. North** received the M.A. degree in natural sciences and computing science from the University of Cambridge, Cambridge, U.K., in 1988, and the D.Phil. degree in three-dimensional computer vision from Sussex University, Sussex, U.K., in 1993.

From 1992 to 2000, he was with the Natural Environment Research Council (NERC), Centre for Ecology and Hydrology. He is currently a Senior Lecturer at the University of Wales Swansea, Swansea, U.K., and a member of the NERC Climate and Land Surface Systems Interaction Centre. His research interests include modeling the interaction of radiation with natural surfaces and retrieval of atmospheric and land surface biophysical information from multidirectional satellite observations.



**Sietse O. Los** received the B.Sc. degree in geology from Rijksuniversiteit Groningen, Groningen, The Netherlands, in 1982, and the M.Sc. and Ph.D. degrees in hydrogeology from Vrije Universiteit, Amsterdam, The Netherlands in 1987 and 1998, respectively.

From 1989 to 2001, he was with the GIMMS group, NASA Goddard Space Flight Center. He is currently a Senior Lecturer at the Department of Geography, University of Wales Swansea, Swansea, U.K., and is the Acting Director of the Natural Environment Research Council Climate and Land-Surface Systems Interaction Centre. His research interests are in satellite-based monitoring of global vegetation and in interactions between vegetation and climate.



**William M. F. Grey** received the B.Sc. degree in geography from the University of Southampton, Southampton, U.K., in 1997, the M.Sc. degree in remote sensing from the University of Dundee, Dundee, U.K., in 1998, and the Ph.D. degree in Earth observation from the University of Wales Swansea, Swansea, U.K., in 2002.

He is currently a Postdoctoral Researcher within the Natural Environment Research Council Climate and Land-Surface Systems Interaction Centre, University of Wales Swansea. His main area of research involves the retrieval of aerosol properties from satellite data.



**Ross M. Mitchell** received the B.Sc. degree in physics and the Ph.D. degree in astrophysics from the University of Melbourne, Melbourne, Australia, in 1975 and 1979, respectively.

After postdoctoral research in astrophysics in the U.K., he joined the CSIRO Division of Atmospheric Research, Canberra, Australia, in 1985, working in the areas of satellite radiometric calibration and atmospheric correction. Since 1997, his work has been focused on the characterization of Australian continental aerosol by combining observations at the surface with satellite retrievals.